Efficient preparation of graphene liquid cell utilizing direct transfer with large-area well-stitched graphene

Yuki Sasaki [a], Ryo Kitaura [a,*], Jong Min Yuk [b,c,d], Alex Zettl [b,c,d], Hisanori Shinohara [a,*]

[a] Department of Chemistry & Institute for Advanced Research, Nagoya University, Nagoya 464-8602, Japan
[b] Department of Physics, University of California at Berkeley, Berkeley, CA 94720, USA
[c] Materials Sciences Division, Lawrence Berkeley National Laboratory, Berkeley, CA 94720, USA
[d] Kavli Energy NanoScience Institute at the University of California, Berkeley and the Lawrence Berkeley National Laboratory, Berkeley, CA 94720, USA

ABSTRACT

By utilizing graphene-sandwiched structures recently developed in this laboratory, we are able to visualize small droplets of liquids in nanometer scale. We have found that small water droplets as small as several tens of nanometers sandwiched by two single-layer graphene are frequently observed by TEM. Due to the electron beam irradiation during the TEM observation, these sandwiched droplets are frequently moving from one place to another and are subjected to create small bubbles inside. The synthesis of a large area single-domain graphene of high-quality is essential to prepare the graphene sandwiched cell which safely encapsulates the droplets in nanometer size.

© 2016 Elsevier B.V. All rights reserved.

1. Introduction

Electron microscope observation of solution and solution-based processes is one of the important issues in nanometer-scale science. For example, the direct structural observation of biomolecules, such as proteins, in water provides crucial information to understand how the protein works in living systems [1–4] and how physical changes occur in solution such as dissolution, precipitation and dispersion [5–7]. Until now, great research efforts have been devoted to elucidate the microscopic structure and dynamics of solution, in which various spectroscopic techniques have been widely employed to obtain information on various phenomena in solutions [8–11].

Observation of solutions using transmission electron microscopy (TEM) can, in principle, provides direct information on microstructure of solution at atomic level [12–18]. Recent advancement on TEM has enabled us to observe structure of matters with spatial and time resolution down to 0.05 nm and 1 ms, respectively [19,20]. In addition, development of low-acceleration voltage technique has greatly expanded versatility of TEM, enabling us to observe bio-organic fragile materials at atomic resolution [21]. High-resolution TEM simultaneously gives us information on electronic structure and bonding state [22]. If

TEM can equally be applied to observe solution, it must be one of the most powerful characterization techniques to provide direct and high-resolution structural information on solution.

TEM observation of solutions have achieved by using environmental cell [23,24]. Recently we demonstrate graphene liquid cells: liquids sandwiched by two single-layer graphene sheets for visualization of metal particles in solution with atomic resolution [16,17,25]. Graphene is the one-atom-thick carbon sheet, and due to the thinnest structure composed of a light element, graphene is almost transparent to electron beam [26,27]. In addition, graphene is a mechanically and chemically stable conductor [28–30], and high-contrast and stable TEM observation can be done using graphene as a sample support [31–33]. In addition, even a single-layer graphene has the perfect impermeability, and if various solutions can be sandwiched between two graphene layers, the solution can be supported stably even under an UHV condition, which provides TEM observations of microstructure of solutions [17,34].

There are, however, some unsavory points corresponding to reproducibility and yield of graphene liquid cells because of vulnerability of low-crystalline graphene sheets. It is important to utilize high-quality graphene to ease the fabrication of the graphene liquid cells as well as of graphene nano-ribbons [34–36].

Here, we have development a simple technique for preparation of the graphene liquid cell by utilizing direct transfer process with large-area and high-quality graphene grown on copper. The large area high-quality graphene was based on the chemical vapor deposition (CVD) on copper foils, which has been developed by

Ruoff and coworkers [37,38]. The pretreatment of copper foils with atmospheric pressure of pure hydrogen gas provides well-stitched and large-area graphene within a relatively short reaction time. By using such a well-stitched graphene and direct transfer process, we are able to prepare the graphene liquid cell in high yield.

2. Materials and methods

We used copper foils as substrates for graphene growth. A copper foil (nilaco, 99.9%, $10 \times 100 \times 0.02$ mm) was placed in a quartz tube and annealed at 1323 K under 500 sccm flow of 100% hydrogen for 50 min [37,39,40]. After the pre-anneal treatment, copper (111) surface preferentially appears. Graphene growth was then performed under 250 sccm flow of $Ar/H_2/CH_4$ (Ar: 97%, H_2: 3%, CH_4: 0.0002%) at the same temperature. The typical growth time of a mm size graphene is ca. 16 hours.

Graphene grown on a copper foil was transferred onto a TEM grid (SiN membrane film with 2 μm pore) using the direct transfer method. To remove copper substrates, a copper foil with a continuous film of graphene grown on the surface was placed on aqueous solution of ammonium peroxodisulfate (1 mol/L) for 12 h (see supplementary information). This process can remove the copper foil almost completely, leading to the graphene film floating on the etching solution, the graphene film was picked up by a SiN TEM grid, and the picked-up graphene was then carefully placed onto aqueous solution of hydrochloric acid to remove copper residues. Before fabrication of a graphene liquid cell, the so-washed graphene on the TEM grid was further cleaned with hydrogen plasma treatment [31,41].

The TEM observation was made with either a field-emission type JEM-2100F or JEM-2010 with an acceleration voltage of 80 kV. Typical exposure time and current density were 0.3 s and 96 A/cm^2, respectively.

3. Results and discussion

Our strategy to prepare the graphene liquid cell is a simple and direct preparation of a sandwiched structure using a high-quality large-area CVD-grown graphene. Figure 1 shows the preparation scheme of the graphene liquid cell. First, a CVD-grown graphene is transferred onto a SiN membrane grid with 2 μm holes penetrating through the membrane. Second, using a mist generator, various
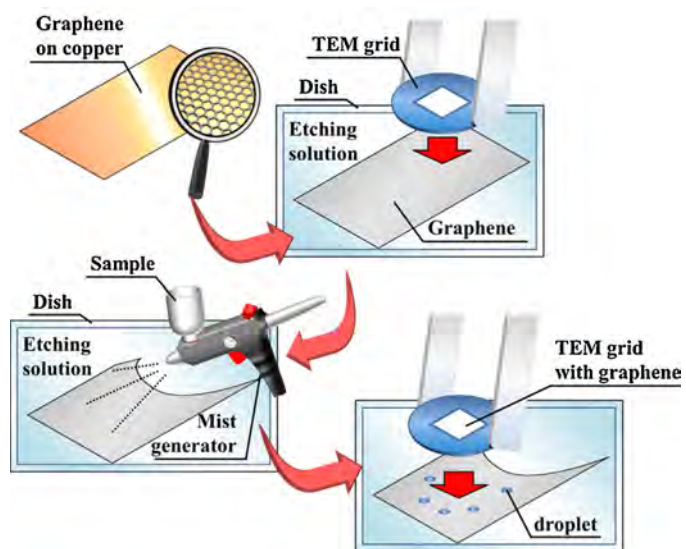

Figure 1. Preparation scheme of the graphene sandwiched structure. Graphene on the solution can be observed by careful irradiation of proper fluorescent light.

solutions are then sprayed onto another graphene specimen floating on etching solution. Third, to form a graphene sandwiched liquid cell, the deposited micro-size droplets of solutions are covered by the originally-transferred graphene on TEM grid. In the preparation of the graphene liquid cell, incorporation of large-area and seamless graphene layers is essential to realize successful encapsulation of solutions. To achieve high-yield preparation of the graphene liquid cell, we have developed a growth technique for high-quality large-area graphene.

Graphene has been synthesized with chemical vapor deposition (CVD) using methane and a cupper foil as the carbon source and the substrate, respectively. The CVD growth of graphene is strongly influenced by the substrate, and (111) plane of cupper has been known as the suitable surface to grow high-quality graphene [42,43]. To prepare the (111) plane, we have utilized high-temperature pretreatment of cupper foil under pure H_2 flow. After the pretreatment, almost all surfaces of the cupper foil have turned into to form (111) plane and grain boundaries in cupper foil have
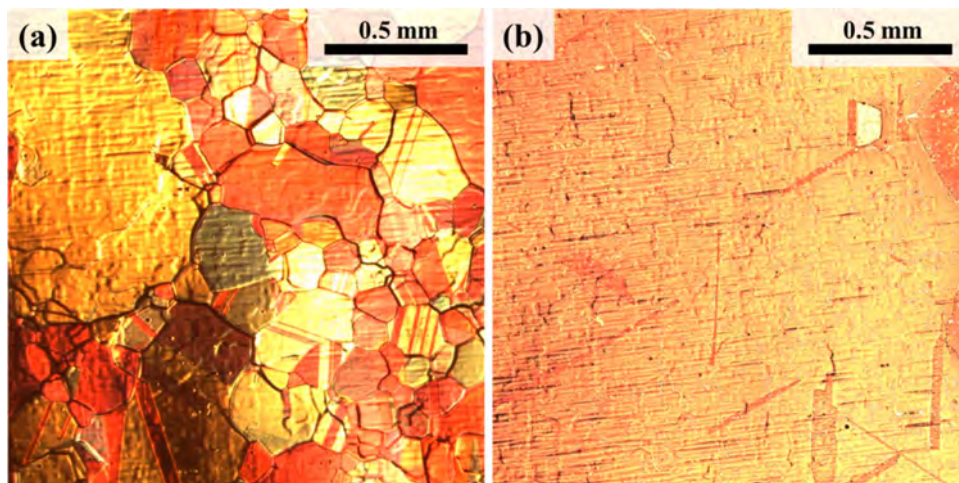
Figure 2. Optical images of copper surface after pretreatment with Ar/H_2 (a) and pure H_2 at high temperatures (b). Both copper surfaces were oxidized by annealing at approximately 500 K to visualize the copper domains and surface orientation via the color variations. Pretreatment for one hour with Ar/H_2 and H_2 at 1327 K results in two quite different surfaces of the copper substrate, as can be seen in (a) and (b): the Ar/H_2 annealed surface has colorful and small copper domains, whereas the pure H_2 annealed surface is simply a flat surface. Because the domain boundaries of the copper surfaces act as nucleation sites for graphene, we never obtain boundary-less graphene sheets for preparing the graphene liquid cells.
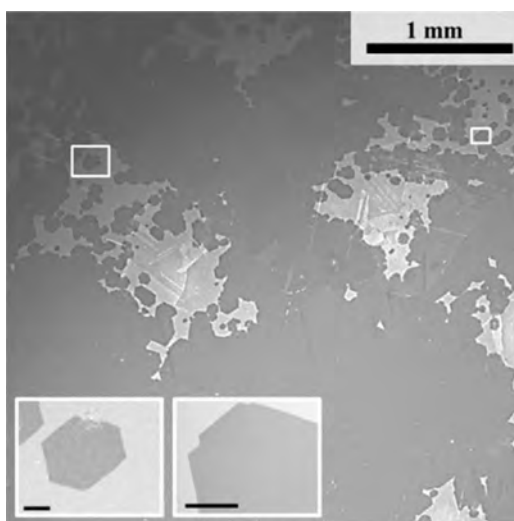
Figure 3. Typical SEM images of single-layer graphene (the dark area) grown on Cu foil annealed in pure H_2 gas. Insert images are zoomed images of the two (white boxed) regions separated about 2 mm. The graphene edges of two images are perpendicular to each other, suggesting that the large area of graphene synthesized maintains high-quality with less grain boundaries. Scale bars in the two insert images are 50 nm.

virtually disappeared, which is different from typical pretreatment using 3% H_2/Ar gas as shown in Figure 2.

Figure 3 shows a typical SEM image of graphene grown on the Cu foil, where hexagonal contrasts due to single-domain graphene are clearly seen. H_2 gas was exchanged to Ar/H_2/CH_4 mixed gases (Ar: 97%, H_2: 3%, CH_4: 0.0002%) to grow graphene and finally it provided large-size orientated mono-layer graphene covered both side of the copper substrate. Raman spectra of the so-prepared graphene show intense G and G' band with an intensity ratio of 1 to 2, which is consistent with monolayer graphene as shown in Figure S1. The Raman spectra were measured after the transfer of the graphene from Cu foil to a SiO_2/Si substrate. Long-time CVD growth of graphene, typically 10 h, using the pretreated cupper foil as a substrate can provide a seamless single sheet of graphene, where the typical size of a grain is about 100 μm^2.

As shown in Figure 3, the mutual orientation of the hexagonal contrasts is unique, indicating that crystal orientation of the present CVD-grown graphene is unique in the area of interest. This unique orientation of the graphene can arise from an epitaxial growth of graphene onto (111) planes of the Cu foil. As shown in Figure 2, Cu foils pretreated using the present method (i.e., the high-temperature pure-H_2 annealing) show Cu (111) surface with a minimal amount of grain boundaries. The present long-time CVD growth with the pretreated Cu foils leads to the formation of well-stitched large-area graphene, which is advantageous to a high-yield preparation of graphene liquid cells. Figure 4a shows a typical TEM image of the current CVD-grow single-layer graphene, whereas Figure 4b exhibits the corresponding electron diffraction pattern, where a hexagonal diffraction spot consistent with a single-layer graphene is clearly seen.

The present preparation of the graphene-liquid cell enables us to investigate TEM structural observations of encapsulated liquids. Figure 5a shows a typical TEM image of a graphene liquid cell using the CVD-grown large-area graphene, where pure water droplet is used as liquid encapsulated between the two single-layers of graphene sheets. The dark contrast region corresponds to the graphene water-sandwiched area with a typical lateral size of 160–300 nm (see supplementary information). An estimated average thickness of the sandwiched region is 10–20 water molecule layers. In terms of EELS measurements (see below), the oxygen peak of droplets is very close to that of bulk water, indicating that the chemical environment around oxygen atoms of the observed nano-droplets is very similar to that of bulk water. Black spots seen in the TEM image are due to Cu nanoparticle residues, which are formed and deposited during the transfer process.

The corresponding electron diffraction pattern shown in Figure 5b exhibits two sets of diffraction patterns with six-fold symmetry, which confirms a successful preparation of the graphene sandwiched structure. The electron diffraction shows diffraction spots originating only from the graphene layers and not from the water droplet, suggesting a liquid state of the droplet. The relative angle of the two hexagonal patterns is about 5°, indicating that two graphene sheets with a relative angle of 5° stack to form the graphene-liquid cell. Relative angles in graphene liquid cells are found to vary from one sample to another due to random stacking caused by the manual stacking procedure used in the present preparation of graphene liquid cells.

Figure 5c shows typical low magnification TEM image of graphene liquid cell. Approximately 35 small droplets are counted in each hole of SiN membrane and near 80% holes are suspended by bilayer graphene and the graphene liquid cells.

To confirm the presence of water droplet in the sandwiched structure, we performed electron energy loss spectroscopy (EELS) measurements for the sandwiched region. Figure 6 shows an EELS
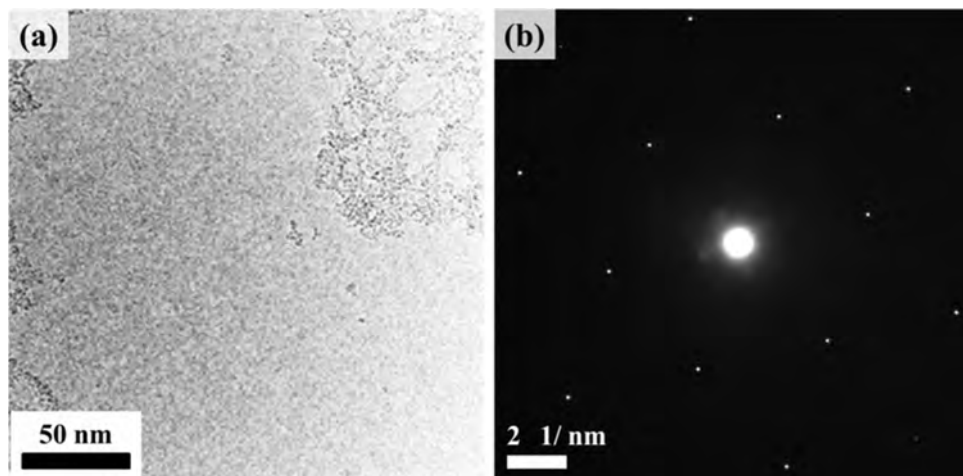
Figure 4. (a) Typical TEM image of the present CVD-grown single-layer graphene. The surfaces are relatively clean except for some amorphous carbon residue (top right) which is attached during the transfer process; (b) the electron diffraction pattern of graphene in (a). A hexagonal pattern indicates the presence of single-layer graphene.
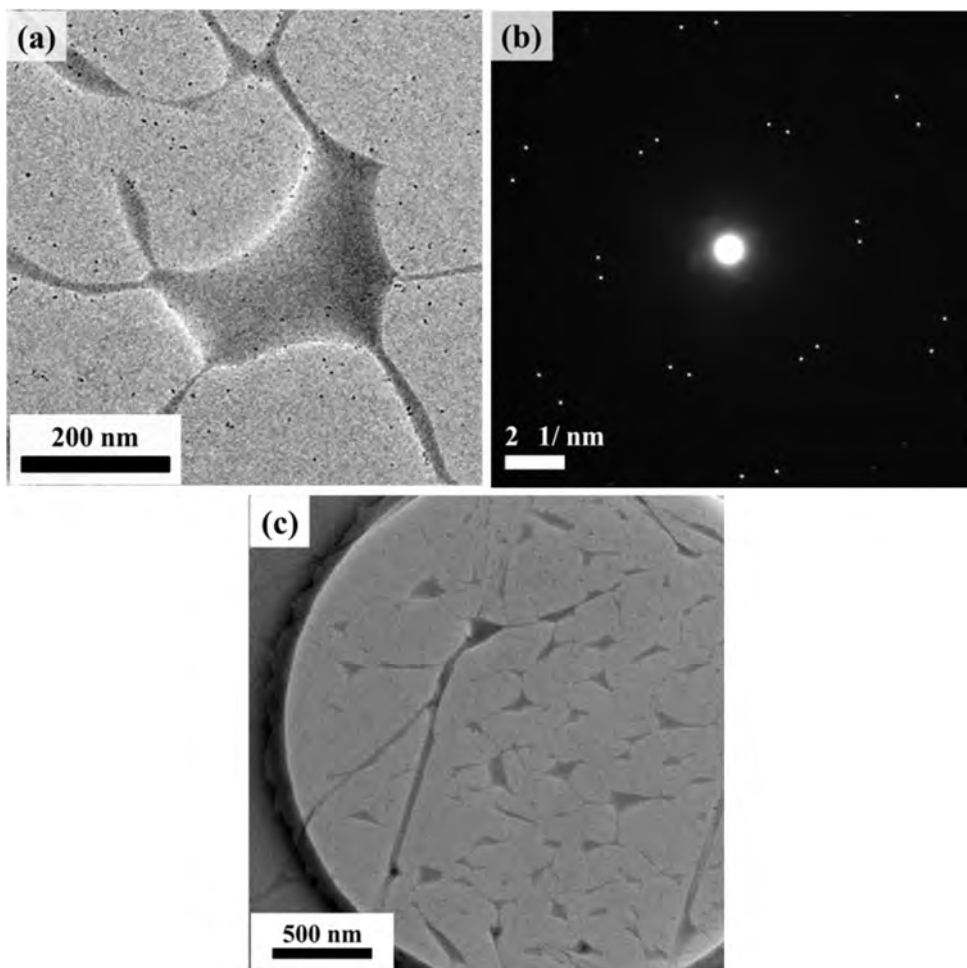
Figure 5. (a) A room temperature typical TEM image of a water-sandwiched area (dark contrast region) by two sheets of single-layer graphene made of Figure 4. Black spots are Cu nanoparticle residues remained, which are formed and deposited during the transfer process; (b) the electron diffraction pattern of graphene water-sandwiched area in Figure 4a. A twin hexagonal patterns shows the graphene sandwiched structure which is made of two sheets of single-layer graphene. (c) Low magnification typical TEM image of the graphene liquid cell. The SiN membrane, which has 2 μm holes, is found in the edge of (c). Many trigonal dark points shown water-encapsulated area is observed in a hole of membrane.
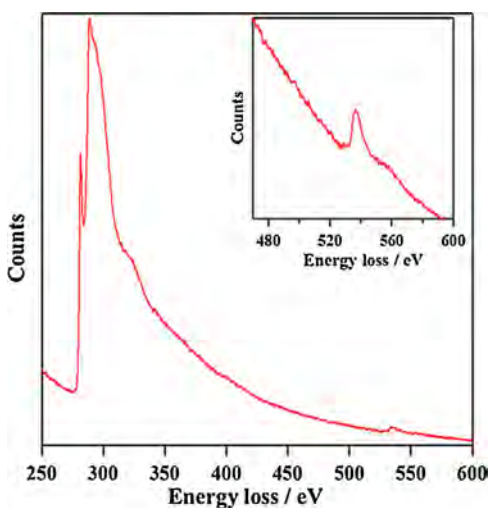
Figure 6. Electron-energy-loss (EELS) spectrum with a selector aperture acquired for the graphene water-sandwiched area in Figure 4. Oxygen K-edge peak (540 eV) due to the sandwiched water droplet is seen together with carbon K-edge peak (284 eV). The inset shows an expanded view of oxygen peak area.

spectrum corresponding to the water sandwiched region shown in Figure 4a. The observed EELS peaks at 284 and 540 eV originate from the core-loss of carbon and oxygen, respectively. The existence of the EELS peak at 540 eV clearly illustrates the successful encapsulation of water molecules between the graphene layers.

Figure 7 shows a time series of magnified TEM images of a sandwiched water droplet at room temperature. Triangular dark contrasts shown in the figure correspond to the water droplet sandwiched between two sheets of graphene. Electron diffraction shows diffraction spots originating only from the graphene layers which is consistent with the liquid state of the encapsulated water. Importantly, the contrast in the water-sandwiched region decreases as time passes due to the increasing extent of decomposition of the water droplet (due to electron beam induced radiolysis) in a graphene pocket. As seen in these TEM images, a bubble corresponding to the circular low contrast area, which presumably is generated by electron beam irradiation, is observed in the sandwiched region (cf. Supplemental Movies 1 and 2). At 252 s, a second (smaller) bubble is appearing in the sandwiched region. These bubbles are frequently observed in water-sandwiched regions during the course of TEM observations. The TEM observation shown here demonstrates that a time-dependent dynamics of liquid water droplets can be observed at nanometer scale using the graphene-sandwiched structure.
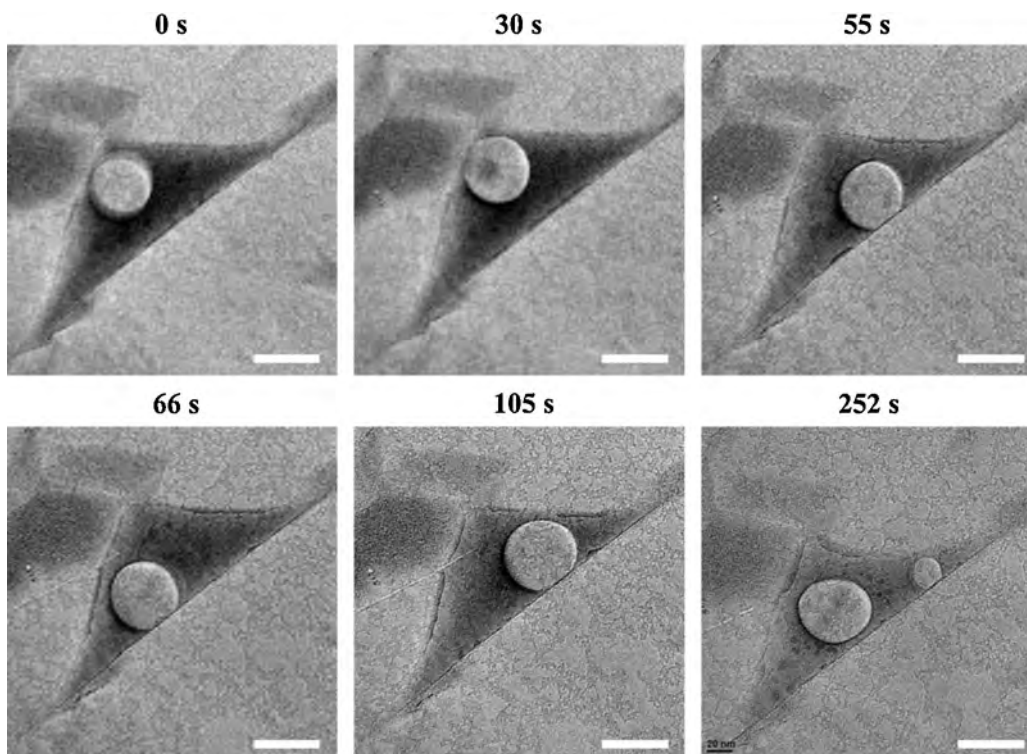
Figure 7. Time series of room temperature TEM images of graphene water-sandwiched region (triangle dark contrast area) at room temperature with a scale bar of 50 nm. A bubble (circular low contrast area), which stems from electron beam irradiation, is also seen in the sandwiched region. The contrast in the water-sandwiched region decreases as time passes due to the increasing decomposition of the water droplet from the interstitial space of the two single-layer graphene. At 252 s, a second (smaller) bubble is appearing in the sandwiched region.

4. Conclusion

Using the TEM and EELS analysis, the present experiments confirm the encapsulation of water nano-droplets between two single-layer graphene sheets. Typically, small sandwiched droplets as small as 100–300 nm in size are observed by TEM. In our preparation, we found the average counts of small droplets is $10.2\,\mu\text{m}^{-2}$ and we confirmed that one TEM grid have approximately 224 000 pockets in our preparation. Direct transferring with spraying the sample mist onto high quality and large size graphene provides high yield of graphene liquid cells. The time-dependent TEM observation often shows a creation of bubbles within the water sandwiched area due to the radiolysis by electron beam irradiation during the observation, which is concomitant with decomposition of the droplets in a graphene pocket.

Acknowledgments

Appendix A. Supplementary data

Supplementary data associated with this article can be found, in the online version, at doi:10.1016/j.cplett.2016.02.066.

References

[1] K.-L. Liu, C.-C. Wu, Y.-J. Huang, H.-L. Peng, H.-Y. Chang, P. Chang, L. Hsu, T.-R. Yew, Lab Chip 8 (2008) 1915.
[2] A.T. Petkova, R.D. Leapman, Z. Guo, W.-M. Yau, M.P. Mattson, R. Tycko, Science 307 (2005) 262.
[3] H.G. Heide, J. Cell Biol. 13 (1962) 147.
[4] D. Parsons, Science 186 (1974) 407.
[5] D. Li, H. Zhou, I. Honma, Nat. Mater. 3 (2004) 65.
[6] R.H. Somani, B.S. Hsiao, A. Nogales, S. Srinivas, A.H. Tsou, I. Sics, F.J. Balta-Calleja, T.A. Ezquerra, Macromolecules 33 (2000) 9385.
[7] J.M. Yuk, H.K. Seo, J.W. Choi, J.Y. Lee, ACS Nano 8 (2014) 7478.
[8] U. Bergmann, P. Wernet, P. Glatzel, M. Cavalleri, L. Pettersson, A. Nilsson, S. Cramer, Phys. Rev. B 66 (2002) 092107.
[9] R. Rosenberg, P. LaRoe, V. Rehn, J. Stöhr, R. Jaeger, C. Parks, Phys. Rev. B 28 (1983) 3026.
[10] N. de Jonge, F.M. Ross, Nat. Nanotechnol. 6 (2011) 695.
[11] H. Zheng, R.K. Smith, Y.-W. Jun, C. Kisielowski, U. Dahmen, A.P. Alivisatos, Science 324 (2009) 1309.
[12] E. Boyes, P. Gai, Ultramicroscopy 67 (1997) 219.
[13] H. Troiani, M. Miki-Yoshida, G. Camacho-Bragado, M. Marques, A. Rubio, J. Ascencio, M. Jose-Yacaman, Nano Lett. 3 (2003) 751.
[14] T. Tsukuda, Bull. Chem. Soc. Jpn. 85 (2012) 151.
[15] M.J. Sharif, M. Yamauchi, S. Toh, S. Matsumura, S.-i. Noro, K. Kato, M. Takata, T. Tsukuda, Nanoscale 5 (2013) 1489.
[16] J.M. Yuk, Q. Zhou, J. Chang, P. Ercius, A.P. Alivisatos, A. Zettl, ACS Nano 1 (2016) 88.
[17] J.M. Yuk, J. Park, P. Ercius, K. Kim, D.J. Hellebusch, M.F. Crommie, J.Y. Lee, A. Zettl, A.P. Alivisatos, Science 336 (2012) 61.
[18] M. Jeong, J.M. Yuk, J.Y. Lee, Chem. Mater. 27 (2015) 3200.
[19] P. Batson, N. Dellby, O. Krivanek, Nature 418 (2002) 617.
[20] R. Beacham, A. Mac Raighne, D. Maneuski, V. O'Shea, S. McVitie, D. McGrouther, J. Instrum. 6 (2011) C12052.
[21] T. Sasaki, H. Sawada, F. Hosokawa, Y. Sato, K. Suenaga, Ultramicroscopy 145 (2014) 50.

[22] A. Bruma, F. Negreiros, S. Xie, T. Tsukuda, R.L. Johnston, A. Fortunelli, Z.Y. Li, Nanoscale 5 (2013) 9620.

[23] H.-G. Liao, D. Zherebetskyy, H. Xin, C. Czarnik, P. Ercius, H. Elmlund, M. Pan, L.-W. Wang, H. Zheng, Science 345 (2014) 916.

[24] J. Wu, W. Gao, J. Wen, D.J. Miller, P. Lu, J.-M. Zuo, H. Yang, Nano Lett. 15 (2015) 2711.

[25] M. Jeong, J.M. Yuk, J.Y. Lee, Chem. Mater. 27 (2015) 3200.

[26] J.C. Meyer, A.K. Geim, M. Katsnelson, K. Novoselov, T. Booth, S. Roth, Nature 446 (2007) 60.

[27] R. Nair, P. Blake, J. Blake, R. Zan, S. Anissimova, U. Bangert, A. Golovanov, S. Morozov, A. Geim, K. Novoselov, Appl. Phys. Lett. 97 (2010) 153102.

[28] C. Lee, X. Wei, J.W. Kysar, J. Hone, Science 321 (2008) 385.

[29] K. Novoselov, A.K. Geim, S. Morozov, D. Jiang, M. Katsnelson, I. Grigorieva, S. Dubonos, A. Firsov, Nature 438 (2005) 197.

[30] G.-H. Lee, R.C. Cooper, S.J. An, S. Lee, A. van der Zande, N. Petrone, A.G. Hammerberg, C. Lee, B. Crawford, W. Oliver, Science 340 (2013) 1073.

[31] Y. Sasaki, R. Kitaura, Y. Yamamoto, S. Arai, S. Suzuki, Y. Miyata, H. Shinohara, Appl. Phys. Express 5 (2012) 065103.

[32] S. Ding, J.S. Chen, D. Luan, F.Y.C. Boey, S. Madhavi, X.W.D. Lou, Chem. Commun. 47 (2011) 5780.

[33] R. Pasricha, S. Gupta, A.K. Srivastava, Small 5 (2009) 2253.

[34] G. Algara-Siller, O. Lehtinen, F. Wang, R. Nair, U. Kaiser, H. Wu, A. Geim, I. Grigorieva, Nature 519 (2015) 443.

[35] H.E. Lim, Y. Miyata, M. Fujihara, S. Okada, Z. Liu, Arifin, K. Sato, H. Omachi, R. Kitaura, S. Irle, K. Suenaga, H. Shinohara, ACS Nano 9 (2015) 5034.

[36] R.R. Meyer, J. Sloan, R.E. Dunin-Borkowski, A.I. Kirkland, M.C. Novotny, S.R. Bailey, J.L. Hutchison, M.L.H. Green, Science 289 (2000) 1324.

[37] X. Li, W. Cai, J. An, S. Kim, J. Nah, D. Yang, R. Piner, A. Velamakanni, I. Jung, E. Tutuc, S.K. Banerjee, L. Colombo, R.S. Ruoff, Science 324 (2009) 1312.

[38] Y. Hao, M.S. Bharathi, L. Wang, Y. Liu, H. Chen, S. Nie, X. Wang, H. Chou, C. Tan, B. Fallahazad, H. Ramanarayan, C.W. Magnuson, E. Tutuc, B.I. Yakobson, K.F. McCarty, Y.-W. Zhang, P. Kim, J. Hone, L. Colombo, R.S. Ruoff, Science 342 (2013) 720.

[39] P. Zhao, A. Kumamoto, S. Kim, X. Chen, B. Hou, S. Chiashi, E. Einarsson, Y. Ikuhara, S. Maruyama, J. Phys. Chem. C 117 (2013) 10755.

[40] G.H. Han, F. Güneş, J.J. Bae, E.S. Kim, S.J. Chae, H.-J. Shin, J.-Y. Choi, D. Pribat, Y.H. Lee, Nano Lett. 11 (2011) 4144.

[41] J. Moser, A. Barreiro, A. Bachtold, Appl. Phys. Lett. 91 (2007) 163513.

[42] Y. Ogawa, B. Hu, C.M. Orofeo, M. Tsuji, K.-i. Ikeda, S. Mizuno, H. Hibino, H. Ago, J. Phys. Chem. Lett. 3 (2012) 219.

[43] S. Ikeda, K. Saiki, Y. Wada, K. Inaba, Y. Ito, H. Kikuchi, K. Terashima, T. Shimada, J. Appl. Phys. 103 (2008) 084313.